26 — 28.09.1995
Sofia
BULGARIA

GENERALIZED THEORY OF GEARING AND ELASTOHYDRODYNAMIC LUBRICATION OF SPUR GEARS

Doctoral Student G. Nikas, Assist. Prof. Dr. Th. Costopoulos
National Technical Univ. of Athens
Greece

SYNOPSIS

The newly developed generalized theory of gearing is used to examine the elastohydrodynamic lubrication of spur-type gears used in power transmission and gear pumps. A forward iterative numerical method is used for the simultaneous solution of the equations governing the complex situation of elastohydrodynamically lubricated teeth of meshing gears. Results received by the present work are in good agreement with those reported by other researchers.

1. INTRODUCTION

Elastohydrodynamic lubrication (EHL) is a form of fluid-film lubrication in which elastic deformation of the lubricated surfaces becomes significant. The complete solution of the general elastohydrodynamic problem requires that parameters like the change of lubriacant' s viscosity and density, due to pressure and temperature, its rheological behaviour, the elastic deformation of the meshing gear teeth, transient effects, surface roughness, effect of heat produced by viscosity on micro-EHL, have to be taken into account. The solution of such a problem becomes difficult mainly because the nonlinear Reynolds' equation is very sensitive to minor errors in measuring the film thickness. In general, there are four types of numerical methods for the solution of EHL problems: Newton-Raphson methods, inverse iterative method, multilevel methods and forward iterative methods Refs.[1] to [8]. Forward iterative methods are the most convenient, although they present problems in case of heavy loads. The numerical method used here is a forward iterative method, which is simple and straightforward. The difficulty of convergence under heavy loads can be eliminated by allowing large number of iterations. According to [1], the minimum film thickness over the whole range of theoretical solutions can be fairly accurately represented by the formula

$$h_{min} = \frac{\mathbf{1.6 \cdot \alpha^{0.6}(u.\eta_0)^{0.7} \cdot (E')^{0.03} \cdot R^{0.43}}}{\mathbf{w^{0.13}}}$$

where **R** is the equivalent radius of local curvature, **E'** is the effective elastic modulus, **u** is the mean of the tangential speeds of the cooperaring surfaces, **w** is the load per unit width, α and η_0 are the viscous properties of the lubricant. This formula is valid for the vast majority of machine elements where contacts are between metal and metal with a film of mineral oil acting as lubricant. From the parameters of this equation, the most influential are **R** and **u**. In case of gears, both quantities **R** and **u** depend on the position of contact which influences also the operational and other parameters of the conjugate gear set. Such parameters are mainly the sliding velocity of the meshing teeth flanks and the tooth compliance. Sliding velocity and accompanying viscous friction force are responsible for the power loss that is transformed to heat, which increases the temperature of the lubricant and influences its viscosity and density. On the other hand, compliance of the meshing teeth has an effect on gear geometry and by that on gear loading and its lubrication. Generalized theory of gearing [9] is a powerful tool that is based on the knowledge of the geometry of the rack that cuts the gear pair and by which the designer knows aforehand, through computer modelling and simulation, all the characteristics of the conjugate gears, such as: **i)** the exact geometry of the gear pair, **ii)** the geometric and kinematic quantities needed for the description of EHL ie. **R**, **u** and **e** (**e** stands for the sliding velocity), **iii)** the position of maximum loading of gear teeth. Actually, after the previous step **ii**, the critical point with the minimum lubricant film $\mathbf{h_{min}}$ may be positioned. This positioning is possible with as much accuracy as the designer wants, since discretization of the gear flank may reach thousands of points and may be done very fast in CPU time of a PC-486. In the analysis to follow we have ignored transient effects as well as the effect of surface roughness. We have examined the iso-thermal situation of a Newtonian lubricant for the case of external and internal gears.

2. GENERALIZED THEORY OF GEARING

Fig.1 shows the rack profile **Y = F(X)** in the coordianate system **(X,Y)**. The origin is at pitch point **P(0,0)**, the **X**-axis coincides with the rack pitch line and positive **X**-axis shows the direction of the rack's motion. In this case, the gear has a clockwise rotation. Point **A(X,Y)** of the rack profile corresponds to point $\mathbf{B(X_{pc}, Y_{pc})}$ of the path of contact and to the point $\mathbf{C(X_1, Y_1)}$ of the gear tooth profile. It is obvious from Fig. 1 that point **A** of the rack profile, moved a distance **K**, and point **B** of the gear tooth profile, rotated through angle (θ), will coincide at point **C** of the path of contact, where also point $\mathbf{(X_2, Y_2)}$ of the cooperating gear will be, after rotation through the angle (θ_2). Hence,

$$\mathbf{X_{pc} = X + K} \quad \text{and} \quad \mathbf{Y_{pc} = Y}$$

The law of gearing states that the common normal to the mating profiles at the point of contact must pass through the pitch point **P(0,0)**. Thus, for α < **0** in the clockwise direction, $\mathbf{\tan(\alpha) = - dX/dY = Y_{pc}/X_{pc}}$.

From the above and from the non-slip rotation of the pitch circles $\mathbf{r_{c1}}$ and $\mathbf{r_{c2}}$ of Fig. 2 it follows that

$$\mathbf{K = - Y \cdot [\, X + Y \cdot dY/dX \,] = \theta \cdot r_{c1} = - s \cdot \theta_2 \cdot r_{c2}}$$

where **s = +1** when gear 2 has external teeth, and **s = —1** when gear 2 has internal teeth. Then the corresponding points $\mathbf{(X_1, Y_1)}$, $\mathbf{(X_2, Y_2)}$ of the meshing gears are given by the following relations

$$\mathbf{X_1 = (X + K) \cdot \cos(\theta) - (Y + r_{c1}) \cdot \sin(\theta)}$$
$$\mathbf{Y_1 = (X + K) \cdot \sin(\theta) + (Y + r_{c1}) \cdot \cos(\theta) - r_{c1}}$$
$$\mathbf{X_2 = (X + K) \cdot \cos(\theta_2) - (Y - s \cdot r_{c2}) \cdot \sin(\theta_2)}$$
$$\mathbf{Y_2 = (X + K) \cdot \sin(\theta_2) + (Y - s \cdot r_{c2}) \cdot \cos(\theta_2) + s \cdot r_{c2}}$$

2.1 Equivalent radius of curvature

The necessary equivalent radius of curvature **R** at the point of contact may be found by the relation

$$R^{-1} = R_1^{-1} \pm R_2^{-1}$$

through the radii of curvature R_1, R_2 of the surfaces in contact, which are such that $R_1 < R_2$. Sign "+" refers to nonconforming contacts (eg. external involute spur gears) whereas sign "—" refers to conforming contacts (eg. internal involute spur gears or external spur gears with a circular-arc profile). These radii of curvature are calculated by the relation

$$R_i = \frac{[(X_i')^2 + (Y_j')]^{3/2}}{|X_i' Y_i'' - X_i' Y_i'|}$$

where **i** = 1 or 2 and having in mind that differentiation for the first and second derivative is taken with respect to **X**. Therefore,

$$X_i' = -[(X + K)\,\theta_i' + Y'] \cdot \sin(\theta_i) + \{1 + K' - [Y - (-1)^j \cdot r_{ci}]\,\theta_i'\} \cdot \cos(\theta_i)$$

$$\begin{aligned} X_i'' = {} & \{[Y - (-1)^j \cdot r_{ci}]\,(\theta_i')^2 - 2\cdot(1 + K')\cdot\theta_i' - \\ & - (X + K)\cdot\theta_i'' - Y''\} \cdot \sin(\theta_i) + \\ & + \{K'' - (X + K)\cdot(\theta_i')^2 - 2\cdot Y_i'\cdot \theta_i' - \\ & - [Y - (-1)^j \cdot r_{ci}]\,\theta_i''\} \cdot \cos(\theta_i) \end{aligned}$$

$$\begin{aligned} Y_i' = {} & \{1 + K' - [Y - (-1)^j \cdot r_{ci}] \cdot \theta_i'\} \cdot \sin(\theta_i) + \\ & + [(X + K)\cdot\theta_i' + Y'] \cdot \cos(\theta_i) \end{aligned}$$

$$\begin{aligned} Y_i'' = {} & \{K'' - (X + K) \cdot (\theta_i')^2 - 2\cdot Y'\cdot \theta_i' - \\ & - [(Y - (-1)^j \cdot r_{ci}]\,\theta_i''\} \cdot \sin(\theta_i) + \\ & + \{2\cdot(1 + K') \cdot \theta_i' + (X + K)\cdot\theta_i'' + Y'' - \\ & - [Y - (-1)^j \cdot r_{ci}^2]\,\theta_i'\} \cdot \cos(\theta_i) \end{aligned}$$

$$K = -(Y \cdot Y' + X),$$

$$K' = -(Y' \cdot Y' + Y \cdot Y'' + 1),$$

$$K'' = -(3 \cdot Y' \cdot Y'' + Y \cdot Y''')$$

$$\frac{\theta_i}{K} = \frac{\theta_i'}{K'} = \frac{\theta_i''}{K''} = \frac{-(-1)^j}{r_{ci}}$$

For pinion: **i = j = 1**. For a cooperating large gear with external teeth: **i = j = 2**.

For a cooperating large gear with internal teeth: **i = 2** and **j = 1**.

2.2. Average and sliding velocities

Fig. 2 shows the geometric and kinematic parameters of the point of contact **E** of two mating external gears with centers at O_1 and O_2. The law of gearing states that the common normal NN to the cooperating flanks passes through the point **C**, which is such that (CO_2/CO_1) = gear ratio. Involutometry and analytical geometry give the following for the radius of curvature ρ_1 and ρ_2 of Fig. 2

$$\rho_i = \frac{|(Y'_1/X'_1) \cdot X_1 - Y_1 + (-1)^j \cdot r_{ci}|}{[(Y'_1/X'_1)^2 + 1]^{1/2}}$$

with **i** and **j** taking values as previously mentioned. For the tangential velocities (along the surface of tooth flanks) Fig. 2 gives $u_i = \omega_i \cdot \rho_i$, where ω represents angular velocity. The mean of the surface velocities of the tooth flanks is $u = (u_1 + u_2)/2$ whereas the sliding velocity is given by $e = |u_1 - u_2|$ and the slide/roll ratio is given by $S_r = e/u$. Again **i** and **j** are used as before.

2.3. Example

As an example let us take the non-trivial case of gears of Ref. [10], in which a method for the reduction of delivery fluctuation of spur gear rotary pumps is proposed. The optimized rack profile consists of eccentric circular tooth flanks as shown in Fig.3, where t_o is the circular pitch, λ is an appropriately defined constant which provides the above-mentioned eccentricity of the circular tooth flanks, and h_k, h_f are the addendum and dedendum respectively. Fig. 4 shows the one-side flank of the rack, pinion 1 and meshing gear 2. They are found through the generalized theory of gearing, as analyzed previously, with the help of the following data: **module = 30 mm**, $h_k = h_f$ = **24.9** mm, number of teeth $Z_1 = Z_2 = 6$, and pinion speed $N_1 = 200$ RPM.

For the use of EHL in these gears, 20 points have been taken on the rack's profile of Fig. 4 and the pertinent points of gears 1 and 2 have been found, as mentioned above. Then, the equivalent radius **R**, the mean velocity **u**, the sliding velocity e and the slide/roll ratio S_r, as given by the previously developed equations, have been caclulated. The results of these calculations, shown if Figs. 5 to 8, have been possible through 500 points of discretization.

3. THE ELASTOHYDRODYNAMIC LUBRICATION PROBLEM

The equations governing the EHL line contact problem are presented for quantities with SI units and they are as follow:

— **Reynolds' equation**. This equation describes the relation between pressure and film shape. For steady-state, one-dimensional flow, it reads as

$$\frac{d}{dx}\left(\frac{\rho \cdot h^3}{\eta} \cdot \frac{dp}{dx}\right) = 12 \cdot u \cdot \frac{d\,(\rho \cdot h)}{dx}$$

with the boundary conditions $p = 0$ at he boundaries $x = x_{in}$ (inlet) and $x = x_{out}$ (outlet), the cavitation condition p 0 and at the outlet $dp/dx \approx 0$ (the approximate equation is due to the fact that Reynolds' equation is not valid at the cavitation boundary).

— **Force balance and film thickness**. Pressure **p** has to be in equilibrium with the externally applied load **w** per unit width of the tooth

$$w = \int_{x_{out}}^{x_{in}} p(s) \cdot ds$$

— **Film thickness** may be determined as follows

$$h(x) = h_o + [x^2/2R] + \upsilon(x)$$

where h_o is an integration constant determined by the force balance and $\upsilon(x)$ represents the elastic deformation of the surfaces.

— **Elastic deformation of the surfaces** given by

$$\upsilon(x) = \frac{2}{\pi \cdot E'} \int_{x_{out}}^{x_{in}} p(s) \cdot \ln(x - s)^2 \cdot ds + c$$

where the integration constant c may be calculated by taking an appropriate datum of displacements. If the materials of the two meshing gears 1 and 2 have Poisson' s ratios ν_1, ν_2 and Young's modulus E_1, E_2 respectively, then the equivalent modulus of elasticity for the gear set is taken as

$$E' = 2/[(1 - \nu_1^2)/E_1 + (1 - \nu_2^2)/E_2]$$

— **Viscosity-pressure relationships**. The dynamic viscosity of the lubricant is found by the relation of Roelands

$$\eta = \eta_o \cdot \exp\{[\ln(\eta_o) + 9.668]\cdot[-1 + (1 + 5.1\cdot10^{-9}\cdot p)^z]\}$$

or by the relation of Barus, for pressure less than approximately 100 N/mm^2, $\eta = \eta_o \cdot \exp(\alpha p)$ where η_o is the viscosity of the lubricant at the conditions of entry (i.e. at surface temperature of the solids at entry and normally at atmospheric pressure). Barus'' piezoviscous coefficient α and constant z of the above equation are connected through Houpert' s relation

$$z = \alpha / \{5.1 \cdot 10^{-9} \cdot [\ln(\eta_o) + 9.668]\}$$

The lubricant's density (neglecting temperature effects) may be found by the relation

$$\rho = \rho_o \cdot [p \cdot 6 \cdot 10^{-10} / (1 + p \cdot 1.7 \cdot 10^{-9}) + 1]$$

where ρ_o is the density of the lubricant at the conditions of entry.

4. CALCULATION OF ELASTIC DEFORMATIONS

The elastic deformations $\upsilon(x)$ may be found by the previously mentiomed equation, if the pressure distribution $p(s)$ is known. A linear pressure distribution $p(s) = a_o + a_1 \cdot s$ is taken as the interpolating polynomial. For a region $[s_1, s_2]$, the integration for $\upsilon(x)$ is carried out and the deformation $\upsilon\{s_1, s_2\}$ is calculated to be such that

$$\upsilon\{s_1, s_2\} = 2 \cdot (a_o \cdot f_o + a_1 \cdot f_1)$$

where variables f_o and f_1 can easily be found.

It is noted that the grid is taken with equal steps Δs (equally spaced mesh). Moreover, the initial node is at the outlet $x = x_{out}$ (that is to say the step $\Delta s = s_2 - s_1$ is negative). The total displacement is the sum of all partial displacements from $s = x_{out}$ to $s = x_{In}$.

5. SOLUTION OF REYNOLDS' EQUATION

Reynolds' equation is solved in three steps:

Step A In the region (x_{out}, x_{spike}), where x_{spike} corresponds to the point of pressure spike, an appropriate discritization of Reynolds' equation gives:

$$p_{i+1} = (A - B)/C \quad \text{for which}$$

$$A = [3\cdot H_i - 4\cdot H_{i-1} + H_{i-2}]\cdot p_{i-1} + 4\cdot H_i\cdot(2\cdot p_i - p_{i-1})$$

$$B = 24u\Delta x[h_i(3\rho_i - 4\rho_{i-1} + \rho_{i-2}) + \rho_i(3h_i - 4h_{i-1} + h_{i-2})]$$

$$C = 7\cdot H_i - 4\cdot H_{i-1} + H_{i-2} \quad \text{and} \quad H = \rho \cdot h^3 / \eta$$

If a pressure spike does not occur, the above procedure is followed up to the inlet x_{In}.

Step B In the region $(x_{spike}, [x]_p)$ between the point of the pressure spike and the point where the pressure becomes less than $p = 100$ N/mm^2, the next equation is used (H as before):

$$p_i = (D + E + F)/G \quad \text{where}$$

$$D = (3H_{i+1} + H_{i-1})\cdot p_{i+1}$$

$$E = (3H_{i-1} + H_{i+1})\cdot p_{i-1}$$

$$F = 24u\Delta x\cdot[(\rho h)_{i+1} - (\rho h)_{i-1}]$$

$$G = 4 \cdot (H_{i+1} + H_{i-1})$$

For the discretization of this region two kinds of nodes are used, i.e. "odd" and "even" nodes. In each iteration of the numerical procedure "odd" and "even" nodes are used alternatively. If the pressure does not become less than 100 N/mm^2, then this step is omitted.

Step C In the area $([x]_p, x_{In})$ Barus' equation is used for calculation of viscosity, although Roelands' equation gives almost the same results. In this case, the first three terms in a Taylor expansion series are used in a step-by-step numerical integration Ref. [1].

Concluding, we may summarize the whole procedure as follows:

(1) The initial pressure distribution is set up as being Hertzian (dry contact). Constant h_o is set up by experience or calculated from its equation, above.

(2) The position x_{out} is evaluated by the boundary conditions there, namely $p = 0$ and $dp/dx = 0$. By using Reynolds' equation in the form

$$dp/dx = 12 \cdot \eta \cdot u \cdot [\rho \cdot h - (\rho \cdot h)_m] / (\rho \cdot h)^3$$

where m denotes the position of maximum pressure, and by applying the boundary conditions we have

$$x_{out} = \{2R \cdot [(\rho \cdot h)_m / \rho_o - h_o]\}^{1/2}$$

As found in previous works, x_{out} is expected to be around (1÷1.2) B where B is the half Hertzian contact width given by the relation

$$B = [8wR / (\pi E')]^{1/2}$$

at load w per unit length.

(3) The elastic deformations are calculated and then the film thickness is found.

(4) For the found film thickness, steps A, B and C are applied and the new pressure distribution is calculated. In step C, point x_{In} is the last point where the pressure is positive (to avoid starvation).

(5) Convergence values for the pressure and film thickness are found. The criterion for pressure convergence is

$$\text{errorp} = \Sigma\, |p - p_{old}| / \Sigma p \langle \text{errpre}$$

and the load criterion is

$$\text{errorw} = \frac{\Delta x}{2\cdot w} \cdot \sum_{i=1}^{N-1} (p_i + p_{i+1}) - 1 \langle \text{errw}$$

where N is the number of nodes and errpre and errw should not exceed a value of 0.05.

(6) Each time, the pressure distribution is revised by letting $p_{new} = 0.3\cdot(p_{old} - p) + p$ where an under-relaxation factor equal to 0.3 is used. Constant h_o is revised by letting $(h_o)_{new} = h_o + 0.24\cdot(w/\pi E')\cdot\text{errorw}$. As an example, and by using the above-mentioned procedure, we may find the pressure distribution as shown in Fig. 9, for which the following data have been taken: $U = (\eta_o u)/(E'R) = 1\cdot10^{-11}$, $W = w/(E'R) = 2.04\cdot10^{-5}$, $G = \alpha E' = 5000$, $u = 0.77$ m/s, $R = 27$ mm, $\eta_o = 0.08$ Pa·s, $\rho_o = 870$ kg/m^3, $\nu_1 = \nu_2 = 0.3$, $\alpha = 2.19\cdot10^{-8}$ Pa^{-1}, $E' = 2.2831\cdot10^{11}$ N/m^2.

The discretization of the region (—B, B) where B is half Hertzian contact width as already mentioned, has been done with 400 equally spaced nodes. The calculated pressure spike is 688 N/mm^2 which is in reasonable agreement with that calculated in [2] for the same data, which was found to be 727 N/mm^2. In that case, Barus' equation was used all along the region (x_{In}, x_{out}) which gives higher values of viscosity and therefore higher pressures than Roelands' equation.

Then, the Example 2.3 is completed with the application of EHL equations on 20 points of a tooth flank. Fig. 10 shows the distribution of maximum pressure values as well as the distribution of minimum film thickness at those 20 points on the gear flanks. The point with critical conditions is easily found in Fig. 10 and it is noted that it corresponds to the 11th point of discretization, whose pressure distribution is given in Fig. 11. The pressure spike is spectacularly present. For the purpose of comparison of pressure distribution between adjacent points, the pressure distribution at the 10th point of gear flank is shown in Fig. 12.

6. DISCUSSION

The theory presented in this paper is a robust mathematical tool for the study of elastohydro-dynamically lubricated spur gears. It is generalized because it can be used in every spur gear geometry. This is very important in an optimization procedure where different gear geometries are to be tested. The benefits of present theory are more obvious in the case of transient EHL (eg. for the study of scuffing and the calculation of flash temperatures due to sliding frictional heating). In that case, the change of film thickness with time depends upon: (1) the change of equivalent radius of curvature with time, (2) the change of average entrainment velocity with time, and (3) the change of teeth pair load with time. Using the present paper, parameters (1) and (2) can easily be calculated. As far as parameter (3) is concerned, the authors would like to mention that they have proposed a method for involute spur gears (see Ref. [11]) and that a paper for the general case of every spur gear geometry is currently under preparation.

REFERENCES

[1] **Dowson, D. and Higginson, G. R.,** *Elastohydrodynamic Lubrication*, Pergamon Press, Oxford, 1977.

[2] **Yang, P. and Wen, S.,** A forward iterative numerical method for steady-state elastohydrodynamically lubricated line contacts, *Tribol. Intern.*,1990.

[3] **Yang, P. and Wen, S.,** A fast, robust straightforward algorithm for thermal elastohydrodynamic lubrication, *Tribol. Intern.*, 1993.

[4] **Johnson, K. L.,** *Contact Mechanics,* Cambridge University Press, Cambridge, 1985.

[5] **Lubrecht, A. A., Ten Napel, W. E. and Bosma, R. Multigrid,** An Alternative Method for Calculating Film Thickness and Pressure Profiles in EHL Line Contacts, *ASME J. Tribology.*, 1986.

[6] **Venner, C. H., Ten Napel, W. E. and Bosma, R.** Advanced Multilevel Solution of the EHL Line Contact Problem, *ASME J. Tribology.*, 1990.

[7] **Glander, D. W. and Bissett, E. J.,** On the Stability and Uniqueness of EHL, *ASME J.Tribology*,1988.

[8] **Ten Napel, W. E. and Yenner, C. H.** Developments in EHL calculations with multilevel techniques,Rolling element bearings - towards the 21st Century, *IMechE,* 1990.

[9] **Costopoulos, Th.,** *Generalized Theory of Gearing and Tooth Stress,* Paper submitted for publication,1993.

[10] **Costopoulos, Th., Kanarachos, A. and Pantazis, E.** Reduction of delivery fluctuation and optimum tooth profile of spur gear rotary pumps, *Mech. Mach. Theory,* 1988.

[11] **Costopoulos, Th. and Nikas, G.,** Minimization of spur gear dynamic loading through the generalized theory of gearing, Paper submitted for publication, 1994.

Assist. Prof. Dr. Th. Costopoulos (*)
Doctoral Student G.K.Nikas (*)
National Technical Univ. of Athens
Department of Mechanical Engineering
Nigritis 4, Athens 11252, Greece

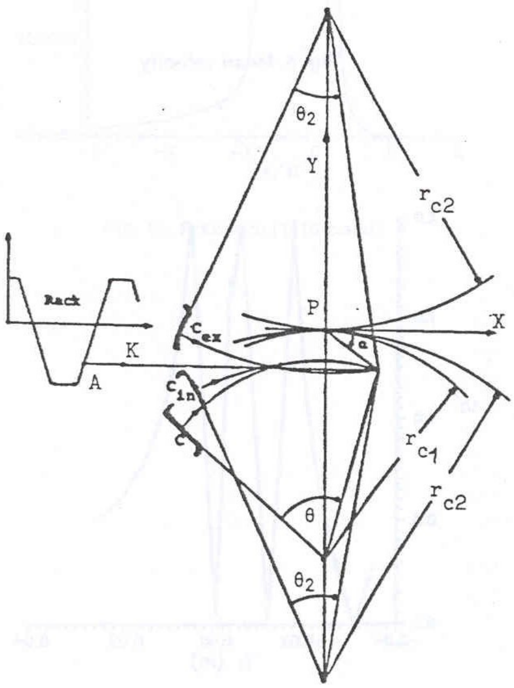

Fig. 1. Generating process of gear flanks

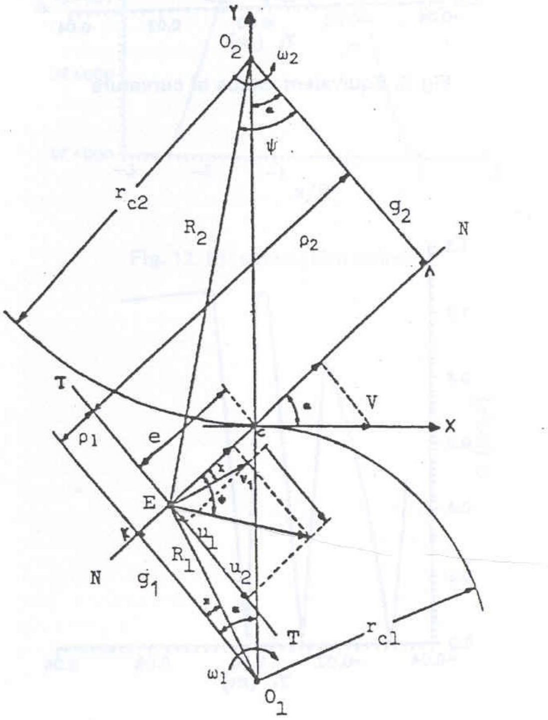

Fig. 2. The law of gearing

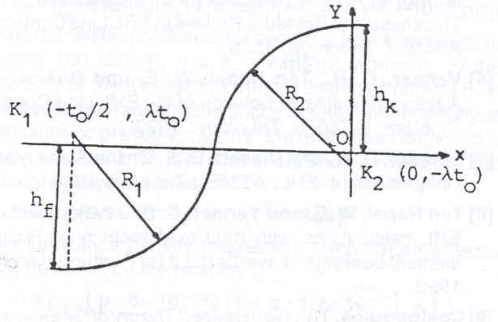

Fig. 3. Eccentric circular tooth flank

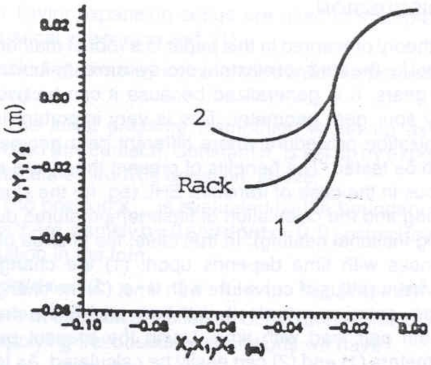

Fig. 4. Tooth profiles

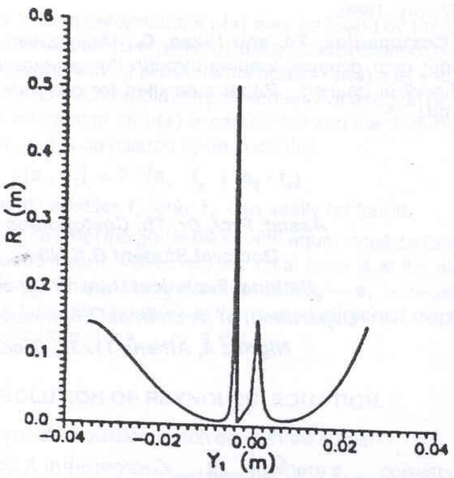

Fig. 5. Equivalent radius of curvature

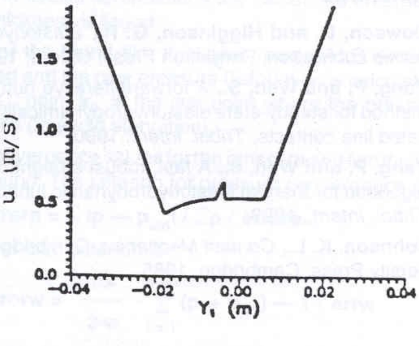

Fig. 6. Mean velocity

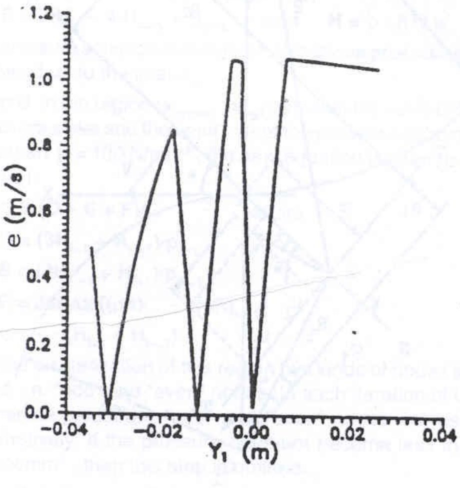

Fig. 7. Sliding velocity

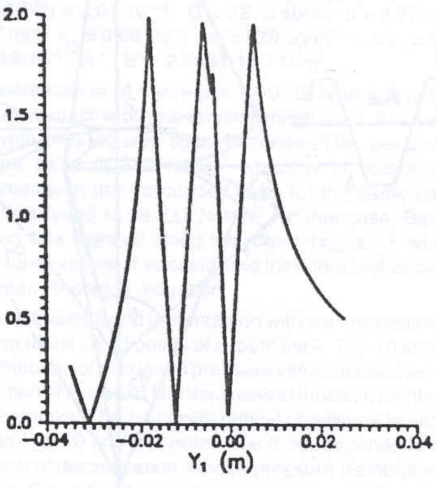

Fig. 8. Slide/roll ratio

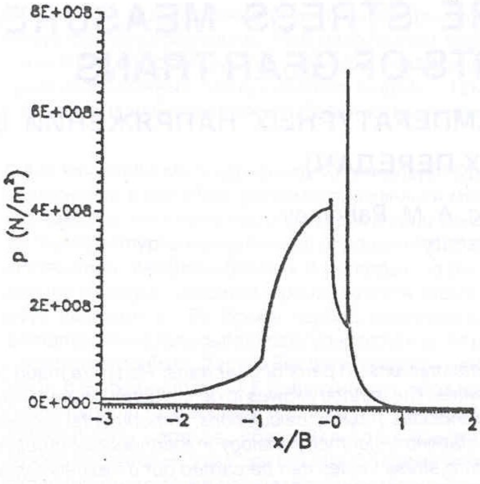

Fig. 9. Pressure distribution

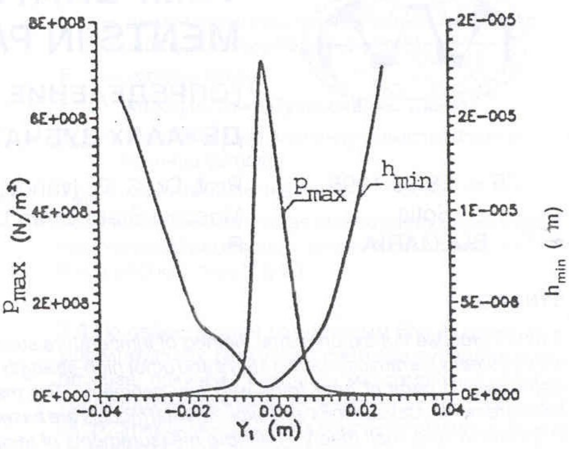

Fig. 10. Max. Pressure and Min. film thickness

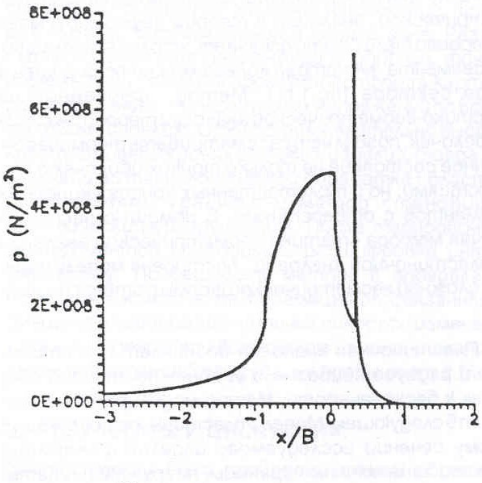

Fig. 11. Pressure (11th point)

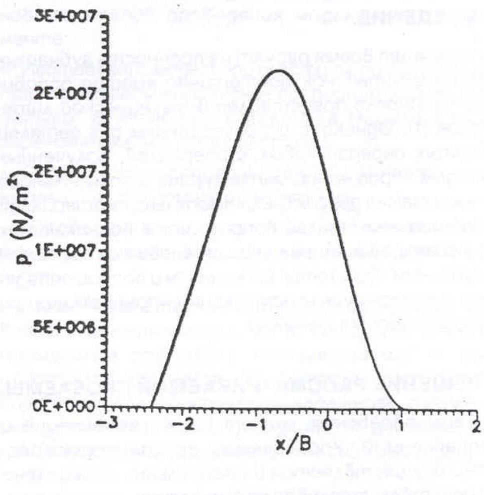

Fig. 12. Pressure (10th point)